nature geoscience

LETTERS

PUBLISHED ONLINE: 22 FEBRUARY 2009 | DOI: 10.1038/NGEO443

Human amplification of drought-induced biomass burning in Indonesia since 1960

Robert D. Field[1]*, Guido R. van der Werf[2] and Samuel S. P. Shen[3]

Much of the interannual variability in global atmospheric carbon dioxide concentrations has been attributed to variability of emissions from biomass burning[1–3]. Under drought conditions, burning in Indonesia is a disproportionate contributor to these emissions, as seen in the 1997/98 haze disaster[1,4]. Yet our understanding of the frequency, severity and underlying causes of severe biomass burning in Indonesia is limited because of the absence of satellite data that are useful for fire monitoring before the mid-1990s. Here we present a continuous monthly record of severe burning events from 1960 to 2006 using the visibility reported at airports in the region. We find that these fires cause extremely poor air quality conditions and that they occur only during years when precipitation falls below a well defined threshold. Historically, large fire events have occurred in Sumatra at least since the 1960s. By contrast, the first large fires are recorded in Kalimantan (Indonesian Borneo) in the 1980s, despite earlier severe droughts. We attribute this difference to different patterns of changes in land use and population density. Fires in Indonesia have often been linked with El Niño[1,2,5–12], but we find that the Indian Ocean Dipole pattern is as important a contributing factor.

The Indonesian haze disaster in 1997/98 (refs 1,4) had pronounced regional impacts on air quality[9]. Average emissions from the region are smaller than those from Africa, but are comparable to emissions from the Amazon basin[4]. As most emissions in Indonesia stem from peat fires and deforestation, with limited forest regrowth, they contribute to the build-up of CO_2 in the atmosphere. Future fire risk in Indonesia will be sensitive to potentially drier conditions[13] and increases in anthropogenic landscape disturbance[14–16].

During 1997–2006, there were two major fire episodes in Indonesia (1997/98, 2006) and two minor episodes (2002, 2004) detected in the Global Fire Emissions Database (GFED; ref. 4), which occurred during droughts of different strengths[12,15]. Before this, there are no high-quality, continuous records of the fires. There are, however, case-by-case accounts of coincident drought and fire years during the 1980s and early 1990s in Indonesia[6], also detected in elevated ozone and aerosol concentrations from the Total Ozone Mapping Spectrometer[5,17], and predominantly linked to El Niño-induced droughts. Fires are observed almost year-round, but the main fire season starts as early as July and lasts until mid-November, typically peaking in September and October.

The Indonesian fires are unique in that the bulk of emissions is due to the continuous burning of peat soils for up to four consecutive months[1], which produces aerosol concentrations high enough to significantly reduce visibility[7,10]. To better understand the severity of biomass burning haze and its underlying causes, we used visibility records from Sumatra and Kalimantan's World Meteorological Organization level meteorological stations to calculate monthly mean extinction coefficients (B_{ext}). Regional mean B_{ext} was computed for Sumatra and Kalimantan, each of which had three stations with data back to 1960 (Fig. 1). We computed B_{ext} using the Koschmeider relationship, omitting observations where present weather codes indicated precipitation or fog (see Supplementary Section S1).

We found an excellent correspondence between regional B_{ext} and TPM estimates from the GFED for both Sumatra ($R^2 = 91$, Fig. 2a,b) and Kalimantan ($R^2 = 0.85$, Fig. 3a,b) for the period of 1997–2006. We note that the two data sources are entirely independent, with the GFED data being derived largely from remote-sensing data and biogeochemical modelling[4], and the B_{ext} being derived from simple meteorological observations at airports. As an indication of the severity of the 1997 haze event and its impact on air quality, the extreme monthly B_{ext} values from stations near the centre of the main burning regions (maximum 16.6 km^{-1}, high values indicating poor visibility) were over five times greater than the extreme monthly B_{ext} values at the cities recognized as having the world's worst air quality (maximum 3.1 km^{-1}) (see Supplementary Table S1).

In Sumatra, the extended B_{ext} data captured events in 1991 and 1994, and to a lesser degree that of 1982 (Fig. 2b). These events were coincident with elevated ozone concentrations detected by the Total Ozone Mapping Spectrometer sensor[5]. There were also large events in 1961, 1963 and 1972 of a slightly lesser magnitude than those in the 1990s, but easily distinguishable from the background B_{ext} level. All events from 1960 to 2006 occurred during periods of anomalously low seasonal rainfall (Fig. 2c).

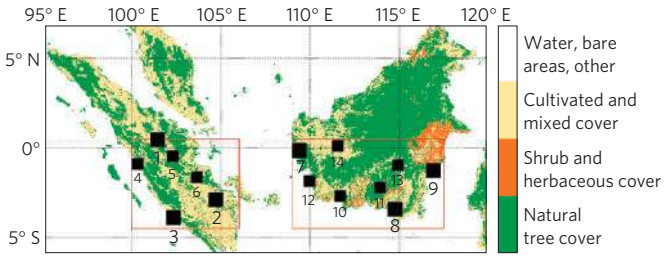

Figure 1 | Land cover from Global Land Cover 2000 (ref. 29) and World Meteorological Organization stations used in the analysis, listed in Supplementary Table S1. Stations 1–3 and 7–9 were used in the long-term analysis. The red boxes outline the regions over which total particulate matter (TPM) emissions, precipitation and population were analysed for Sumatra (0.5° N–4.5° S, 100° E–106° E) and Kalimantan (0.5° N–4.5° S, 109° E–117.5° E).

[1]Department of Physics, University of Toronto, Toronto, M5S 1A7, Canada, [2]Faculty of Earth and Life Sciences, VU University Amsterdam, Amsterdam, 1081HV, Netherlands, [3]Department of Mathematics and Statistics, San Diego State University, San Diego 92182, USA. *e-mail: robert.field@utoronto.ca.

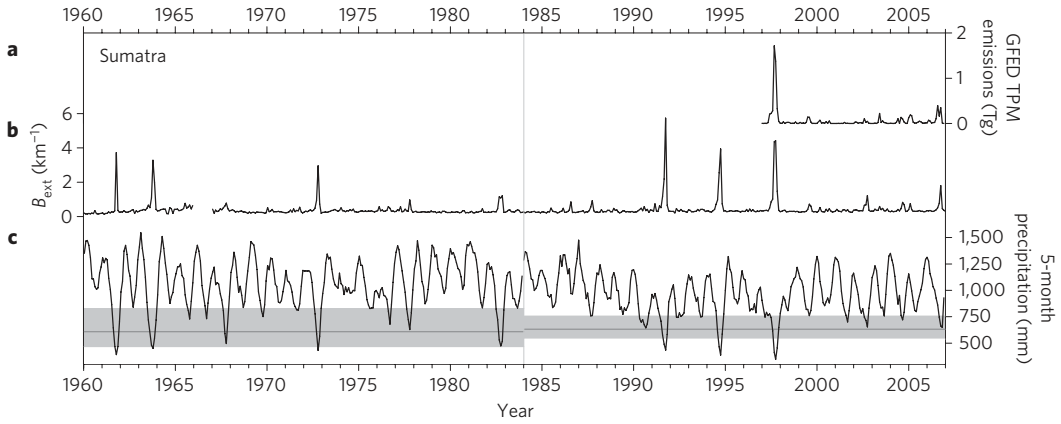

Figure 2 | Monthly time-series for Sumatra. a, GFED TPM emission estimates[4], **b**, mean B_{ext}, and **c**, five-month back-totalled precipitation from the NCEP Precipitation over Land (PRECL) data[27] for 1960–1983 and the Global Precipitation Climatology Project[28] for 1984–2006. The grey vertical line separates the two analysis periods. The grey horizontal lines in **c** show the estimated precipitation threshold α during each period, and the shading shows the 95% confidence interval for α. Supplementary Fig. S1 shows the B_{ext} and precipitation data in a scatter-plot view. See the Methods section for a description of the precipitation data and threshold definition.

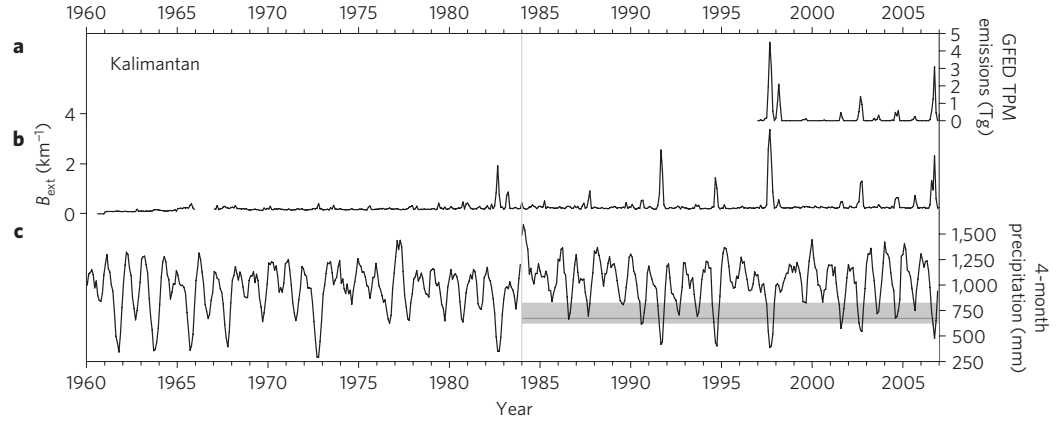

Figure 3 | Monthly time-series for Kalimantan. a, GFED TPM emission estimates[4], **b**, mean B_{ext}, and **c**, four-month back-totalled PRECL precipitation for 1960–1983 and Global Precipitation Climatology Project precipitation for 1984–2006. The grey vertical line separates the two analysis periods. The grey horizontal line in **c** shows the estimated precipitation threshold α during 1984–2006, and the shading shows the 95% confidence interval for α. No threshold is shown for 1960–1983, owing to the poor fit of the model. Supplementary Fig. S2 shows the B_{ext} and precipitation data in a scatter-plot view. See the Methods section for a description of the precipitation data and threshold definition.

Conversely, severe events were absent during non-drought years, despite regular dry seasons.

We estimated the nonlinear relationship between precipitation and haze using piecewise linear regression, splitting the data into an early period (1960–1983) and recent period (1984–2006) to detect any possible changes in the sensitivity of fire to drought. The piecewise model includes a threshold parameter α, which separates normal precipitation conditions from those under which severe haze is possible (see the Methods section). We considered back-totalled precipitation of between 2 and 6 months as predictor variables, selecting the back-totalling period that yielded the highest coefficient of determination R^2 as optimal.

In Sumatra during 1960–1983, five-month back-totalled precipitation was the best predictor, explaining 67% of the variance in B_{ext} over Sumatra, with a threshold of 609 mm (see Supplementary Table S2, Fig. 2c). Below this threshold, there was a sensitivity of $-0.011\,km^{-1}\,mm^{-1}$, indicating an increase in B_{ext} with decreasing precipitation (see Supplementary Fig. S1a). During the 1984–2006 period, five-month precipitation could explain 85% of the variance in B_{ext}, with a threshold of 631 mm and a below-threshold sensitivity of $-0.015\,km^{-1}\,mm^{-1}$ (see Supplementary Fig. S1b). The improved predictability during the 1984–2006 period can be attributed in part to the higher-quality precipitation data during that period (see the Methods section), and perhaps to a slightly stronger sensitivity of the Sumatran fire environment to drought.

In Kalimantan, there was a very different history of biomass burning. Severe haze events under drought conditions are evident from 1982 onwards, but unlike those in Sumatra were largely absent during the 1960s and 1970s (Fig. 3b). Atmospheric trajectory analysis showed that the absence of haze during this period was not attributable to differences in wind flow (see Supplementary Section S2). The 1972 and 1997 droughts, for example, had similar patterns of atmospheric transport between the burning region and the visibility stations, but severe haze was observed only in 1997 (see Supplementary Section S2). There is anecdotal evidence of the 1972 haze event being present over Borneo[11], but the absence of the event in the B_{ext} record indicates that it was of a much smaller magnitude than subsequent events, consistent with the absence of fire in East Kalimantan in 1972 (ref. 8).

More quantitatively, the four-month precipitation was the best predictor during 1984–2006 over Kalimantan, explaining 78% of the variance in B_{ext}, with a precipitation threshold of 672 mm and a below-threshold sensitivity of $-0.007\,km^{-1}\,mm^{-1}$

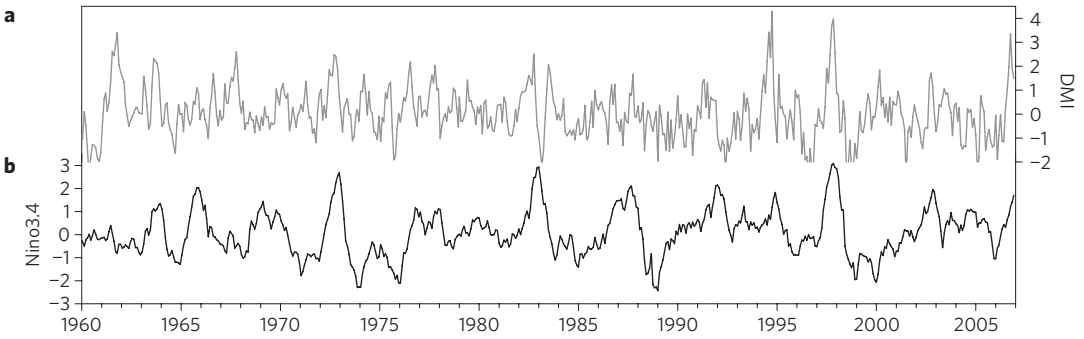

Figure 4 | SST time series. a, Dipole mode index (DMI; ref. 19) and **b**, Nino3.4 index calculated from the Smith and Reynolds global gridded SST analysis[30]. The Nino3.4 index is defined as the standardized SST anomaly over the 5° S–5° N and 170° W–120° W region of the Pacific Ocean. The DMI is defined as the difference of the SST anomalies between the western equatorial Indian Ocean (50° E–70° E, 10° S–10° N) and the southeastern equatorial Indian Ocean (90° E–110° E, 10° S–0° N).

(see Supplementary Table S2, Fig. 3, Supplementary Fig. S2a). In contrast, such a relationship was absent from 1960–1983, with only 13% of the variance in B_{ext} explained by the four-month precipitation, and a below-threshold sensitivity of $-0.001\,km^{-1}\,mm^{-1}$, which was not statistically distinguishable from zero (see Supplementary Fig. S2b). Whereas in Sumatra there was only a small increase in fire sensitivity to drought, the Kalimantan fire environment changed from highly fire resistant to highly fire prone at some point between the droughts of 1972 and 1982.

Drought acts as the trigger for fire occurrence, but it is humans who ignite the fires. How do we explain the difference in the evolution of the fire environments in Sumatra and Kalimantan since the 1960s?

In Indonesia, fire is used primarily to clear vegetation waste, and is closely associated with deforestation and agricultural expansion[6,8,11]. The number of ignitions depends on the extent of these activities, which also tend to lower the resilience of tropical forests to drought through changes in moisture balance[8]. Indonesia's overall annual deforestation rate from 1950 to 1997 was 1.1%, but from 1950 to 1985 the deforestation rate in Kalimantan (0.7%) was half that of Sumatra (1.4%). It was only during 1985 to 1997 that the deforestation rate in Kalimantan (2.2%) began to approach that of Sumatra (2.6%) (see Supplementary Section S3).

Kalimantan's later deforestation is characteristic of broader development patterns, reflected by trends in population and agriculture. Sumatra had population densities more than three times greater than Kalimantan during the first half of the twentieth century (see Supplementary Fig. S3). During the 1960s and 1970s, population growth in Sumatra accelerated rapidly, but lagged behind in Kalimantan, approaching Sumatra's 1960s growth rates only in the 1980s. This difference in population growth between the two regions was in part due to the Indonesian government's policy of transmigration to ease population pressure on Java and, later, to develop Indonesia's remote forested regions. Sumatra was the main target region of transmigration through the 1960s and 1970s, whereas Kalimantan became a significant target region only in the 1980s (see Supplementary Section S4). In Kalimantan, the effects of this population shift on land-cover change were exacerbated by a change in focus from small-scale subsistence agriculture to large-scale industrial agriculture and agro-forestry, which have larger land-use footprints. Peatlands drained under the Mega Rice Project of the 1990s, for example, were the single biggest contributor to emissions across all of Indonesia during the 1997 fire event (see Supplementary Section S3).

Overall, we attribute the difference in evolution of Sumatra's and Kalimantan's fire environments to different patterns of human activity and government policy. Fire has been used for millennia in Indonesia[18], but in the past at a much smaller scale[11]. Much of Kalimantan remained relatively undeveloped until the 1980s, which explains the previous absence of major fire events in the B_{ext} record, despite several severe droughts in the 1960s and 1970s.

In addition to their different development patterns, precipitation over Sumatra and Kalimantan is influenced by different patterns of zonal circulation in the tropics. Whereas haze events have been attributed predominantly to El Niño conditions, there is strong evidence that the Indian Ocean Dipole (IOD) also contributes independently to drought over Indonesia[19,20], and was linked to the 1997 fire event[17,21]. Physically, a combination of local and remote forcings contribute to reduced precipitation over Indonesia. Anomalously cool sea surface temperatures (SSTs) in surrounding seas suppress local convection, but, in combination with warm SST anomalies in the western Indian and eastern Pacific Oceans, also reduce moisture convergence over Indonesia[22,23]. Under El Niño or IOD conditions, this effect strengthens into September[20], as moisture over western Indonesia is transported westward to the Indian Ocean[23].

We examined the influence of the El Niño–Southern Oscillation (ENSO) and IOD specifically over the main burning regions in Fig. 1, comparing the regional precipitation variance explained by the Nino3.4 index and DMI as indicators of ENSO and IOD strength, respectively (Fig. 4). Linear correlations were computed during the July–November period when most burning occurs, and over the entire NCEP PRECL data period of 1948–2006. Over Sumatra, the Nino3.4 SST index could explain 30% of the variability in mean July–November precipitation under a linear model, compared with 61% explained by the DMI. A simple index consisting of the sum of the DMI and the Nino3.4 also explained 61% of the variability in Sumatra precipitation, yielding no improvement over the DMI alone. Over Kalimantan, the Nino3.4 could explain 58% of the variability in precipitation, compared with 49% explained by the DMI, but a combined index could explain 72% of the variability. The strength of these controls was somewhat sensitive to the period analysed, definition of season and particular dataset used, but typically either the DMI or combined Nino3.4–DMI index performed better than the Nino3.4 (see Supplementary Section S5).

It is therefore important that SST anomalies over both the Pacific and Indian Oceans be monitored in preventing and mitigating future fire events. Although the 1994 and 2006 events, for example, did occur during moderate El Niño conditions, it was the positive IOD conditions that distinguished them from 2002, when the drought and haze were weaker (Fig. 4). The 1961 event occurred under neutral ENSO and strongly positive IOD conditions, and the severity of the 1997 event seems to be attributable to the combined strength of the El Niño and the IOD.

With the presence of intensive land-use, severe fire years have occurred when seasonal precipitation was below a given threshold, owing to either or both El Niño and positive IOD conditions. Our precipitation threshold estimates can therefore serve as benchmarks

to identify periods of severe haze risk, aiding in the interpretation of seasonal rainfall outlooks for operational fire management.

Such mitigation measures are particularly important under a changing climate, given the possibility of more persistent El Niño-like conditions[24], reduced rainfall over Indonesia's main burning regions[13] and a positive feedback between reduced soil moisture and reduced precipitation in Indonesia[25]. Among countries with humid tropical forests, Indonesia's current deforestation rate of 3.4% per year is second only to that of Brazil[26]. The extent of large-scale oil palm plantations is projected to increase, partly to meet growing demand for biofuels[14]. As droughts are inevitable and may become more severe, Indonesia's future fire regime depends strongly on the extent of these types of human activity.

Methods

For each region, we considered back-totalled rainfall of up to six months as predictor variables. More sophisticated drought indices were not considered, having been shown for 1997–2006 not to provide any advantage over simple rainfall totals[15]. We used the best available precipitation data for each of the 1960–1983 and 1984–2006 analysis periods. The PRECL dataset[27] beginning in 1948 was used for the 1960–1983 period, but was found to have a much more sparse gauge observation network from the 1980s onwards (see Supplementary Fig. S4). For the 1984–2006 period, we therefore used data from the Global Precipitation Climatology Project[28], which blends satellite and rain gauge observations and covers 1979–present.

We used piecewise regression to estimate the nonlinear relationship between precipitation and B_{ext} (ref. 15). This technique provided an explicit estimate of precipitation threshold, and of the sensitivity of B_{ext} to changes in precipitation below this threshold. Physically, the use of a threshold-based model corresponds to moisture ignition thresholds of fuels, particularly in drained peatland[15]. The model consists of two linear segments, constrained to be equal at an unknown threshold α, and is given by

$$B_{ext} = \begin{cases} \beta_0 + \beta_1 x & x \leqslant \alpha \\ \beta_0 + \beta_1 x + \beta_2 (x - \alpha) & x > \alpha \end{cases}$$

where β_0 is the y intercept, β_1 is the slope of the line below α, $\beta_1 + \beta_2$ is the slope of the line above α and x is a given predictor variable, for example, five-month back-totalled precipitation. The below-threshold slope β_1 quantifies the degree to which B_{ext} varies with precipitation. Across the different back-totalling periods, we assessed goodness of fit using R^2, and provide 95% confidence intervals for all estimated parameters using fully paired bootstrapping with 2,000 re-samples. For each of Sumatra and Kalimantan, the back-totalling period yielding the largest R^2 under the piecewise model was selected for interpretation. Scatter-plot versions of Figs 2 and 3 are shown in Supplementary Figs S1,S2, which emphasize the structure of the piecewise model.

Visibility data used in the analysis can be obtained from the US National Climatic Data Center at: http://www.ncdc.noaa.gov/oa/visibility/.

Received 23 October 2008; accepted 27 January 2009; published online 22 February 2009

References

1. Page, S. E. *et al.* The amount of carbon released from peat and forest fires in Indonesia during 1997. *Nature* **420**, 61–65 (2002).
2. van der Werf, G. R. *et al.* Continental-scale partitioning of fire emissions during the 1997 to 2001 El Nino/La Nina period. *Science* **303**, 73–76 (2004).
3. Langenfelds, R. L. *et al.* Interannual growth rate variations of atmospheric CO_2 and its delta C_{13}, H_2, CH_4, and CO between 1992 and 1999 linked to biomass burning. *Glob. Biogeochem. Cycles* **16**, doi:10.1029/2001gb001466 (2002).
4. van der Werf, G. R. *et al.* Interannual variability in global biomass burning emissions from 1997 to 2004. *Atmos. Chem. Phys.* **6**, 3423–3441 (2006).
5. Kita, K., Fujiwara, M. & Kawakami, S. Total ozone increase associated with forest fires over the Indonesian region and its relation to the El Niño-Southern oscillation. *Atmos. Environ.* **34**, 2681–2690 (2000).
6. Bowen, M. R., Bompard, J. M., Anderson, I. P., Guizol, P. & Gouyon, A. in *Forest Fires and Regional Haze in Southeast Asia* (eds Eaton, P. & Radojevic, M.) 41–66 (Nova Science, 2001).
7. Heil, A. & Goldammer, J. G. Smoke-haze pollution: A review of the 1997 episode in Southeast Asia. *Regional Environ. Change* **2**, 24–37 (2001).
8. Siegert, F., Ruecker, G., Hinrichs, A. & Hoffmann, A. A. Increased damage from fires in logged forests during droughts caused by El Nino. *Nature* **414**, 437–440 (2001).
9. Kunii, O. *et al.* The 1997 haze disaster in Indonesia: Its air quality and health effects. *Arch. Environ. Health* **57**, 16–22 (2002).
10. Wang, Y. H., Field, R. D. & Roswintiarti, O. Trends in atmospheric haze induced by peat fires in Sumatra Island, Indonesia and El Nino phenomenon from 1973–2003. *Geophys. Res. Lett.* **31**, doi:10.1029/2003GL018853 (2004).
11. Aiken, S. R. Runaway fires, smoke-haze pollution, and unnatural disasters in Indonesia. *Geogr. Rev.* **94**, 55–79 (2004).
12. Logan, J. A. *et al.* Effects of the 2006 El Nino on tropospheric composition as revealed by data from the Tropospheric Emission Spectrometer (TES). *Geophys. Res. Lett.* **35**, doi:10.1029/2007GL031698 (2008).
13. Li, W. H. *et al.* Future precipitation changes and their implications for tropical peatlands. *Geophys. Res. Lett.* **34**, doi:10.1029/2006GL028364 (2007).
14. Fargione, J., Hill, J., Tilman, D., Polasky, S. & Hawthorne, P. Land clearing and the biofuel carbon debt. *Science* **319**, 1235–1238 (2008).
15. Field, R. D. & Shen, S. S. P. Predictability of carbon emissions from biomass burning in Indonesia from 1997 to 2006. *J. Geophys. Res.* **113**, doi:10.1029/2008jg000694 (2008).
16. van der Werf, G. R. *et al.* Climate regulation of fire emissions and deforestation in equatorial Asia. *Proc. Natl Acad. Sci. USA* **105**, 20350–20355 (2008).
17. Thompson, A. M. *et al.* Tropical tropospheric ozone and biomass burning. *Science* **291**, 2128–2132 (2001).
18. Anshari, G., Kershaw, A. P. & van der Kaars, S. A late Pleistocene and Holocene pollen and charcoal record from peat swamp forest, Lake Sentarum Wildlife Reserve, West Kalimantan, Indonesia. *Paleogeogr. Paleoclimatol. Paleoecol.* **171**, 213–228 (2001).
19. Saji, N. H., Goswami, B. N., Vinayachandran, P. N. & Yamagata, T. A dipole mode in the tropical Indian Ocean. *Nature* **401**, 360–363 (1999).
20. Hong, C. C., Lu, M. M. & Kanamitsu, M. Temporal and spatial characteristics of positive and negative Indian Ocean dipole with and without ENSO. *J. Geophys. Res.* **113**, doi:10.1029/2007JD009151 (2008).
21. Abram, N. J., Gagan, M. K., Mcculloch, M. T., Chappell, J. & Hantoro, W. S. Coral Reef death during the 1997 Indian Ocean dipole linked to Indonesian Wildfires. *Science* **301**, 952–955 (2003).
22. Hendon, H. H. Indonesian rainfall variability: Impacts of ENSO and local air–sea interaction. *J. Clim.* **16**, 1775–1790 (2003).
23. Juneng, L. & Tangang, F. T. Evolution of ENSO-related rainfall anomalies in Southeast Asia region and its relationship with atmosphere-ocean variations in Indo-Pacific sector. *Clim. Dyn.* **25**, 337–350 (2005).
24. Vecchi, G. A. & Soden, B. J. Global warming and the weakening of the tropical circulation. *J. Clim.* **20**, 4316–4340 (2007).
25. Notaro, M. Statistical identification of global hot spots in soil moisture feedbacks among IPCC AR4 models. *J. Geophys. Res.* **113**, doi:10.1029/2007JD009199 (2008).
26. Hansen, M. C. *et al.* Humid tropical forest clearing from 2000 to 2005 quantified by using multitemporal and multiresolution remotely sensed data. *Proc. Natl Acad. Sci. USA* **105**, 9439–9444 (2008).
27. Chen, M. Y., Xie, P. P., Janowiak, J. E. & Arkin, P. A. Global land precipitation: A 50-Yr monthly analysis based on gauge observations. *J. Hydrometeorol.* **3**, 249–266 (2002).
28. Adler, R. F. *et al.* The Version-2 Global Precipitation Climatology Project (GPCP) monthly precipitation analysis (1979-Present). *J. Hydrometeorol.* **4**, 1147–1167 (2003).
29. Stibig, H. J. *et al.* A land-cover map for South and Southeast Asia derived from SPOT-VEGETATION data. *J. Biogeogr.* **34**, 625–637 (2007).
30. Smith, T. M. & Reynolds, R. W. Extended reconstruction of global sea surface temperatures based on COADS data (1854–1997). *J. Clim.* **16**, 1495–1510 (2003).

Acknowledgements

We thank W. Spangler at the National Center for Atmospheric Research for assistance in processing the visibility data, C. Hong for assistance with Supplementary Section S5 and N. MacKendrick, K. Moore and B. de Groot for helpful reviews. R.D.F. was supported by a Natural Sciences and Engineering Research Council of Canada scholarship, and G.R.v.d.W. by a Veni grant from the Netherlands Organization for Scientific Research.

Author contributions

R.D.F. conceived of the study and conducted the data analysis under the graduate supervision of S.S.P.S. All authors contributed to interpretation of the results and writing of the manuscript.

Additional information

Supplementary Information accompanies this paper on www.nature.com/naturegeoscience. Reprints and permissions information is available online at http://npg.nature.com/reprintsandpermissions. Correspondence and requests for materials should be addressed to R.D.F.

SUPPLEMENTARY INFORMATION
DOI: 10.1038/NGEO443

Human amplification of drought-induced biomass burning in Indonesia since 1960

R. D. Field[1], G. R. van der Werf[2], S.S.P. Shen[3]

1. Department of Physics, University of Toronto, Toronto, Canada

2. Faculty of Earth and Life Sciences, VU University Amsterdam, Amsterdam, Netherlands

3. Department of Mathematics and Statistics, San Diego State University, San Diego, United States

Supplementary information

DOI: 10.1038/NGEO443

1. Visibility data

Because of its importance in navigation, visibility has been recorded at World Meteorological Organization (WMO)-level stations throughout the world, and used to identify, for example, long-term temporal improvements in air quality over the eastern US associated with reductions in SO_2 emissions [31], the opposite phenomenon in China's industrial heartland [32,33], and the impact of dust on visibility during dry periods in North Africa and China [34].

Visibility observations are made at ground level using landmarks at known distances without the aid of optical devices, and using point light sources at night [35]. Distances are measured in increments proportional to their magnitude: in 100m steps between 100m and 5000m, in steps of 1km between 6km and 30km, and steps of 5km between 30km and 70km [35]. Visibility observations were obtained from the synoptic meteorological observations in the ds463.0 and ds463.3 archives at the US National Center for Atmospheric Research (NCAR). Over time, there was an increase in the number of hours at which observations were reported. To avoid introducing a diurnal bias over time, we analyzed only the standard 00 and 12 UTC observations, which corresponded to 07:00 and 19:00 local time. Following standard practice, records where the visibility could have been affected by fog or precipitation, and not smoke haze, were excluded [34,36], based on the values of the present weather codes in the synoptic records.

Extinction coefficient (B_{ext}) was calculated from the visibility observations using the Koschmeider relationship [36]:

$$B_{ext} = \frac{K}{V}$$

where K is the Koschmeider constant and V is the visibility in km. The Koschmeider constant K corresponds to the contrast sensitivity threshold of the observer and the inherent contrast between visibility targets and the background sky. We used K=1.9, following previous studies [31,36].

Physically, B_{ext} measures the degree to which visible light is attenuated with distance due to aerosol absorption and scattering, and has units of km^{-1}. Instances of 0m-visibility under extreme haze conditions were replaced with 100 m, the next smallest increment at which visibility is recorded. This makes the B_{ext} used in this analysis conservative during periods of severe haze. For each month, data from the stations across each of Sumatra and Kalimantan were pooled and used to calculate a monthly regional mean. In this way, stations with fewer observations in a given month were not over-represented in the regional signal. In Pontianak, all 00 UTC values from 1960-1964 were missing present weather codes, and so were replaced with the 03 UTC values, when present weather codes were available.

There were six stations in Sumatra and eight stations in Kalimantan, but only three stations in each region had continuous data as far back as 1960 (Figures S5 – S8). The additional stations in Sumatra appear to have been operational in the early 1960s, but much of the data was missing. Conversely, most of the stations in Kalimantan's main burning region appear to have been commissioned only in the 1980s. Interestingly, the availability of this data is due to new airport construction in more remote areas, reflecting

DOI: 10.1038/NGEO443

the population growth and development which contributed to the increased severity of the fire problem. These newer stations were therefore excluded from the long-term signal, to avoid artificially inflating the magnitude of the B_{ext} signal during the 1980s and 1990s.

The B_{ext} signal over Kalimantan is an excellent indicator in distinguishing the magnitudes of the 1997, 2002 and 2006 events, when burning was concentrated in the region bounded by the stations. There was also a significant burning event in early 1998 appearing in the Kalimantan TPM signal, which occurred exclusively in the province of East Kalimantan [4] under localized drought conditions [15,37]. This event is captured only weakly by the long-term B_{ext} signal for Kalimantan (Figure 3 c), which reflected the detection of the event at the Balikpapan station (966330). The event was also strongly evident at the Muaratewe station (965950) (Figure S8), which was directly downwind of East Kalimantan, but whose observations began only in 1984 and were excluded from the long term signal. The Borneo mega-fires of early 1983 [38] occurred under similar drought conditions, and were detected most clearly in the Balikpapan records.

The additional stations also helped to understand the unprecedented severity of the 1997 event, not only in terms of greenhouse gas emissions [5], but also with respect to regional air pollution. For comparison, we considered the B_{ext} extremes in the five major cities recognized as having the world's worst air quality in terms of particulate matter [39]. Indeed, these cities typically had poorer average air quality than the stations in Indonesia, judging by their mean B_{ext} values (Table S1). The extreme events in Indonesia, however, were far worse. Of the five major cities, the highest B_{ext} was 3.1 km^{-1} in Delhi, India,

during December 1998, followed by 1.9 km^{-1} in Chongqing, China, in November 2004. In Sumatra, the highest B_{ext} was 16.6 km^{-1} in Jambi in October of 1997, and in Kalimantan, the highest B_{ext} was 14.1 km^{-1} in Muaratewe in September of 1997, both roughly five times greater than in Delhi.

2. Trajectory analysis

We conducted atmospheric trajectory simulations for Pontianak (965810), Banjarmasin (966850) and Balikpapan (966330) to determine if the absence of haze in the 1960s and 1970s in the Kalimantan B_{ext} data could be explained not by the absence of smoke emissions, but rather by differences in atmospheric flow. Back-trajectories from these locations were computed using the HYbrid Single-Particle Lagrangian Integrated Trajectory (HYSPLIT) model [40], and the wind fields from the NCAR-NCEP Reanalysis [41]. Back trajectories were run from 500m above ground level using a 1-hour time step, for 96 hours in length, for each day in the 1960-2006 period. The eastern region outlined in Figure 1 was identified as the potential source region over Kalimantan.

The absence of haze in the 1960s and 1970s at the Kalimantan stations could not be explained by different patterns of wind flow. At the Pontianak station in West Kalimantan, for example, air masses consistently arrived from the southern Kalimantan burning region in 1972, similar to the haze event of 1997 (Figure S9). Any significant burning emissions during the 1972 drought would have been detected in Pontianak. Banjarmasin in South Kalimantan province lies at the eastern edge of the main burning region, during which the atmospheric flow is from the east. Like Pontianak, there was little difference in the direction of flow between the 1972 and 1997 events (Figure S10).

DOI: 10.1038/NGEO443

More quantitatively, we tracked the number of monthly back-trajectory points which fell within the Kalimantan burning region, as an indicator of the potential source strength over time. To determine if there was a difference between the droughts during the 1960-1983 (1961, 1963, 1965, 1967, 1972, 1982) and 1984-2006 (1987, 1991, 1994, 1997, 2002, 2006) periods, we compared the number of trajectory crossings during the dry months of July-November. In Pontianak, an average of 49.5% (σ = 13.8) of the trajectory points fell within the burning regions during the droughts of 1960-1983, compared to 51.9% (σ = 15.8) during the droughts of 1984-2006, which were not statistically different using a two-sided t-test (p =0.54). In Banjarmasin, an average of 13.5% (σ = 10.1) of the trajectory points fell within the burning regions during 1960-1983, compared to 15.2% (σ = 11.5) during 1984-2006, also not statistically different using a two-sided t-test (p =0.55). In Balikpapan, an average of 9.3% (σ = 9.1) of the trajectory points fell within the burning regions during 1960-1983, compared to 13.1% (σ = 11.6) during 1984-2006, again not statistically different using a two-sided t-test (p =0.17). We further note that the weaker absolute magnitudes of the B_{ext} signal in Banjarmasin and Balikpapan (Figure S8) reflects their location at the upwind extent of Kalimantan's main burning region.

3. Deforestation and peatland drainage

Forest cover estimates for 1950, 1985 and 1997 (Table S3) were used to calculate annual rates of deforestation q using

$$q = \left(\frac{A_2}{A_1} \right)^{1/(t_2 - t_1)} - 1$$

where A_2 and A_1 are the forest cover at t_1 and t_2 [42, 43]. The rapid increase in deforestation rates for both regions corresponds to a substantial increase in logging, with log production increasing in the 1970s by a factor of five from 5 000 000 m^3 in the 1960s to over 25 000 000 m^3 in the 1980s [42]. There was also a significant growth in land allocated for agricultural and estate crops, with oil palm plantations in particular exhibiting rapid expansion in the late 1980s [42,44].

Perhaps the single biggest contributor to Kalimantan's increase in fire sensitivity was the Mega Rice Project (MRP) in Central Kalimantan. Starting in 1995, an area of almost one million ha was cleared from peat swamp forest, and over 4400 km of drainage canals were constructed to make the land suitable for rice agriculture. The peat conditions were unsuitable for rice cultivation, and the sole legacy of the project was one million ha of drained peatlands no longer resilient to drought, and vulnerable to carbon release from oxidation [45] and fire. The MRP area was in fact the single biggest contributor to Indonesia's unprecedented emissions in 1997 from biomass burning, which constituted to up to 40% of annual global fossil fuel emissions at that time [5].

4. Population growth and transmigration

Transmigration had occurred for over a century in Indonesia [46], but its importance increased in the 1960s under the Suharto government, with financial aid from international donors [47]. Sumatra was the main target region of transmigration in earlier stages, due to already established populations and easier access from Java [46], which is separated by only 25 km of sea at its nearest point. From 1951-1969, 83% of transmigrants were settled in Sumatra, compared to 11% in Kalimantan [48]. From 1969 to

DOI: 10.1038/NGEO443

1974, Sumatra continued to be the primary destination (58%), although the proportion destined for Kalimantan had increased to 15%, with a greater emphasis on Sulawesi (26%). At the end of the third phase of planned transmigration in 1984, 62% of families settled in Sumatra, compared to 19% in Kalimantan. The first World Bank-sponsored transmigration phase which explicitly included Kalimantan was initiated only in 1983 [46]. During the 1984/5 to 1988/9 phase, Kalimantan became the planned primary target (42%), with Sumatra a secondary target (27%) [49], although it was not clear whether this reversal had been achieved [50].

At the same time Kalimantan was included as a target region in the 1980s, the focus of the transmigration program shifted from small-scale subsistence farming to large-scale industrial agriculture such as rubber, oil palm, and forest plantations for fuel, pulp and plywood [44,46,48,51]. This shift can result in an increase in per capita land use, for example from 2-5 ha/family for agriculture compared to 20 ha/family for silviculture, as reported for Thailand [52], amplifying the impact in Kalimantan of newly arriving populations.

5. Circulation controls on precipitation over Indonesia

We calculated the Niño 3.4 and Dipole Mode Indices (DMI) using the Smith and Reynolds global gridded SST data [30]. The Niño 3.4 index is defined as the standardized SST anomaly over the 5S-5N and 170W-120W region. The DMI is defined as the difference of the SST anomalies between the western equatorial Indian Ocean (50E-70E, 10S-10N) and the southeastern equatorial Indian Ocean (90E-110E, 10S-0N) [19]. We standardized the DMI to have a variance of 1 in order to construct the simple combined index of Nino3.4 and DMI.

Over Sumatra, the DMI was the best predictor for all PRECL cases considered, typically exceeding the variance explained by the Nino3.4 by a factor of two (Table S4). During the full 1948-2006 PRECL period considered, the DMI could explain 61% of the variance in the precipitation over Sumatra, compared to 30% by the Nino3.4. The combined index also explained 61% of the variance in Sumatra precipitation, offering no improvement over the DMI alone. The relative superiority of the DMI decreased during the 1984-2006 period, when the DMI, Nino3.4 and combined indices explained 72%, 53% and 78% of the Sumatran PRECL precipitation respectively. Using the higher-quality GPCP dataset for 1984-2006 reduced the DMI-Nino3.4 difference even further to 50% and 49% respectively, with a combined index explaining 59% of the variance.

Over Kalimantan, the Nino3.4 was the best predictor for the majority of PRECL cases considered, although the differences between that and the DMI R^2 were smaller than for Sumatra (Table S5). In fact, during the 1960-1983 period, the DMI was the better predictor, and the combined index had an R^2 of 0.80. Further seasonal separation showed that the influence of the Nino3.4 is more dominant during JJA, but that the DMI is actually the stronger predictor during SON.

DOI: 10.1038/NGEO443

Supplementary References

31 Schichtel, B.A., Husar, R.B., Falke, S.R., & Wilson, W.E., Haze trends over the United States, 1980-1995. *Atmos. Environ.* **35**, 5205-5210 (2001).

32 Qian, Y. & Giorgi, F., Regional climatic effects of anthropogenic aerosols? The case of southwestern China. *Geophys. Res. Lett.* **27**, 3521-3524 (2000).

33 Che, H.Z., Zhang, X.Y., Li, Y., Zhou, Z.J., & Qu, J.J., Horizontal visibility trends in China 1981-2005. *Geophys. Res. Lett.* **34**, doi:10.1029/2007GL031450 (2007).

34 Mahowald, N.M., Ballantine, J.A., Feddema, J., & Ramankutty, N., Global trends in visibility: implications for dust sources. *Atmospheric Chemistry and Physics* **7**, 3309-3339 (2007).

35 World Meteorological Organization, Guide to Meteorological Instruments and Methods of Observation *World Meteorological Organization* Report No. 92-63-16008-2, 1996.

36 Husar, R.B., Husar, J.D., & Martin, L., Distribution of continental surface aerosol extinction based on visual range data. *Atmos. Environ.* **34**, 5067-5078 (2000).

37 Field, R.D., Wang, Y., Roswintiarti, O., & Guswanto, A drought-based predictor of recent haze events in western Indonesia. *Atmos. Environ.* **38**, 1869-1878 (2004).

38 Malingreau, J.P., Stephens, G., & Fellows, L., Remote-sensing of forest-fires - Kalimantan and North-Borneo in 1982-83. *Ambio* **14**, 314-321 (1985).

39 World Bank, 2007 World Development Indicators, *World Bank*, 2007.

40 Draxler, R.R. & Hess, G.D., An overview of the Hysplit_4 modelling system for trajectories, dispersion and deposition. *Australian Meteorological Magazine* **47**, 295-308 (1998).

41 Kalnay, E. *et al.*, The NCEP/NCAR 40-year reanalysis project. *Bulletin of the American Meteorological Society* **77**, 437-471 (1996).

42 FWI/GFW,The State of the Forest: Indonesia *Forest Watch Indonesia and Global Forest Watch.*, 2002.

43 Puyravaud, J.P., Standardizing the calculation of the annual rate of deforestation. *For. Ecol. Manage.* **177**, 593-596 (2003).

44 Gellert, P.K., A brief history and analysis of Indonesia's forest fire crisis. *Indonesia* **65**, 63-85 (1998).

45 Hooijer, A., Silvius, M., Wösten, H., & Page., S.,PEAT-CO2, Assessment of CO2 emissions from drained peatlands in SE Asia *Delft Hydraulics* Report No. Q3943, 2006.

46 Fearnside, P.M., Transmigration in Indonesia: lessons from its environmental and social impacts. *Environ. Manage.* **21**, 553-570 (1997).

47 Indonesia transmigration program:A review of five bank supported projects *World Bank*, 1994.

48 Suratman & Guiness, P., The changing focus of transmigration. *Bulletin of Indonesia Economic Studies* **13**, 78-101 (1977).

49 Hardjono, J., Transmigration: looking to the future. *Bulletin of Indonesia Economic Studies* **22**, 28-53 (1986).

50 Leinbach, T.R., The transmigration programme in Indonesian national development strategy: current status and future requirements. *Habitat International* **13**, 81-93 (1989).

51 Barber, C.V. & Schweithelm, J.,Trial by fire: Forest fires and forestry policy in Indonesia's era of crisis and reform *World Resources Institute*, 2000.

52 Lohmann, L., Commercial tree plantations in Thailand: Deforestation by any other name. *The Ecologist* **20**, 9-17 (1990).

53 Klein Goldewijk, K., Estimating global land use change over the past 300 years: The HYDE Database. *Global Biogeochemical Cycles* **15**, 417-433 (2001).

DOI: 10.1038/NGEO443

Supplementary Tables

Table S1. Descriptors and summary B_{ext} statistics for 1973-2006 for Indonesian stations 1 – 14 plotted in Figure 1. The last five stations are those for cities identified as having the world's worst air quality, in terms of PM_{10} [39].

Map ID	WMO Station ID	Station Name	Elevation (m)	Latitude	Longitude	Mean B_{ext} (km^{-1})	Max B_{ext} (km^{-1})	Month of Maximum
1	961090	PAKANBARU	31	0.5	101.5	0.5	7.6	September 1997
2	962210	PALEMBANG	10	-2.9	104.7	0.5	9.5	October 1991
3	962530	BENGKULU	16	-3.9	102.3	0.3	2.7	October 1991
4	961630	PADANG	30	-0.9	100.4	0.2	2.5	September 1997
5	961710	RENGAT	46	-0.5	102.3	0.6	13.1	October 1997
6	961950	JAMBI	25	-1.6	103.7	0.6	16.6	October 1997
7	965810	PONTIANAK	3	-0.2	109.4	0.4	5.9	September 1994
8	966850	BANJARMASIN	20	-3.4	114.8	0.3	3.9	August 1997
9	966330	BALIKPAPAN	30	-1.3	116.9	0.2	2.4	October 1997
10	966450	PANGKALANBUN	25	-2.7	111.7	0.5	11.6	Octoboer 1997
11	966550	PALANGKARAYA	27	-2.2	113.9	0.7	11.6	September 1997
12	966150	KETAPANG	9	-1.9	110.0	0.4	8.3	October 1997
13	965950	MUARATEWE	60	-1.0	114.9	0.6	14.1	September 1997
14	965590	SINTANG	30	0.1	111.5	0.5	13.5	September 1997
	623660	CAIRO, EGYPT	740	30.1	31.4	0.4	1.6	September 1984
	421820	DELHI, INDIA	2160	28.6	77.2	0.9	3.1	December 1998
	428090	CALCUTTA, INDIA	60	22.7	88.5	0.8	1.4	August 2005
	545270	TIANJIN, CHINA	50	39.1	117.2	0.2	0.8	January 1964
	575150	CHONG-QING, CHINA	3510	29.5	106.5	0.6	1.9	November 2004

Table S2. Linear piecewise regression estimates, with 95% confidence intervals in parentheses. The parameter α is the rainfall threshold below which haze events tended to occur. The parameter β_1 is the below-threshold slope, or rate at which B_{ext} changes when precipitation is less than α. Confidence intervals were estimated using fully-paired bootstrapping with 2000 re-samples.

		1960-1983 (PRECL)		1984-2006 (GPCP)	
Sumatra (5-month precipitation)	R^2	0.67	(0.39, 0.88)	0.85	(0.68, 0.93)
	α (mm)	609	(468, 826)	631	(538, 756)
	β_0 ($km^{-1}mm^{-1}$)	6.9	(1.8, 22.2)	9.8	(5.6, 15.7)
	β_1 ($km^{-1}mm^{-1}$)	-0.011	(-0.046, -0.002)	-0.015	(-0.026, -0.007)
	β_2 ($km^{-1}mm^{-1}$)	0.010	(0.002, 0.046)	0.015	(0.008, 0.029)
Kalimantan (4-month precipitation)	R^2	0.13	(0.02, 0.39)	0.78	(0.60, 0.90)
	α (mm)	524	(254, 1893)	672	(616, 822)
	β_0 ($km^{-1}mm^{-1}$)	0.8	(0.2, 5.6)	5.1	(2.8, 7.4)
	β_1 ($km^{-1}mm^{-1}$)	-0.001	(-0.013, 0.000)	-0.007	(-0.011, -0.003)
	β_2 ($km^{-1}mm^{-1}$)	0.001	(0.000, 0.013)	0.007	(0.003, 0.011)

DOI: 10.1038/NGEO443

Table S3. Forest cover estimates (in hectares) for Indonesia, Sumatra and Kalimantan, from the Government of Indonesia and World Bank (GOI-WB), and the Global Forest Watch of the World Resources Institute (GFW-WRI) [42].

	Indonesia		Sumatra		Kalimantan	
Year	GOI-WB	GFW-WRI	GOI-WB	GFW-WRI	GOI-WB	GFW-WRI
1950	162 290 000	162 290 000	37 370 000	37 370 000	51 400 000	51 400 000
1985	119 700 500	117 191 550	22 323 500	22 938 825	39 986 000	39 644 025
1997	100 000 000	95 628 800	16 632 143	16 430 300	31 512 208	29 637 475

DOI: 10.1038/NGEO443

Table S4. R^2 **values for the DMI, Nino3.4 and combined SST indices and precipitation over the boxed region over Sumatra in Figure 1.**

		JUL-NOV			JJA			SON		
Period	**Dataset**	**DMI**	**NINO3.4**	**COMBINED**	**DMI**	**NINO3.4**	**COMBINED**	**DMI**	**NINO3.4**	**COMBINED**
1948-2006	**PRECL**	0.61	0.30	0.61	0.33	0.22	0.46	0.53	0.27	0.51
1960-2006	**PRECL**	0.67	0.35	0.65	0.37	0.32	0.54	0.58	0.26	0.53
1960-1983	**PRECL**	0.65	0.19	0.53	0.43	0.27	0.51	0.54	0.12	0.40
1984-2006	**PRECL**	0.72	0.53	0.78	0.42	0.39	0.61	0.66	0.49	0.66
1984-2006	**GPCP**	0.50	0.49	0.59	0.38	0.43	0.61	0.34	0.34	0.41

Table S5. R^2 **values for the DMI, Nino3.4 and combined SST indices and precipitation over the boxed region over Kalimantan in Figure 1.**

		JUL-NOV			JJA			SON		
Period	**Dataset**	**DMI**	**NINO3.4**	**COMBINED**	**DMI**	**NINO3.4**	**COMBINED**	**DMI**	**NINO3.4**	**COMBINED**
1948-2006	**PRECL**	0.49	0.58	0.72	0.18	0.49	0.48	0.51	0.48	0.63
1960-2006	**PRECL**	0.52	0.62	0.73	0.15	0.51	0.45	0.56	0.53	0.68
1960-1983	**PRECL**	0.64	0.59	0.80	0.36	0.49	0.56	0.65	0.53	0.78
1984-2006	**PRECL**	0.52	0.67	0.71	0.10	0.57	0.40	0.55	0.54	0.65
1984-2006	**GPCP**	0.57	0.67	0.75	0.21	0.57	0.52	0.53	0.47	0.58

DOI: 10.1038/NGEO443

Supplementary Figures

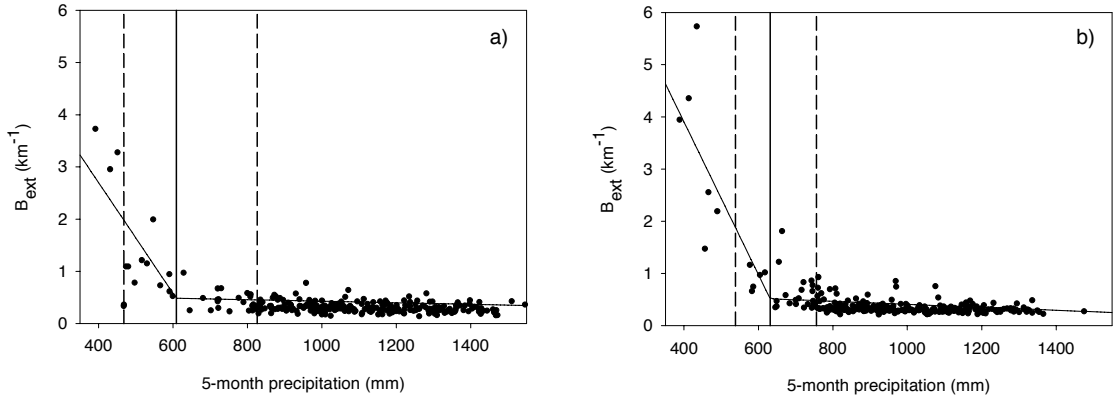

Figure S1. Sumatra piecewise regression fits for a) 1960-1983 and b) 1984-2006. The solid vertical lines show the threshold estimate and the dashed lines show 95% confidence intervals. This is the same data as in Figure 2, but in a scatterplot view.

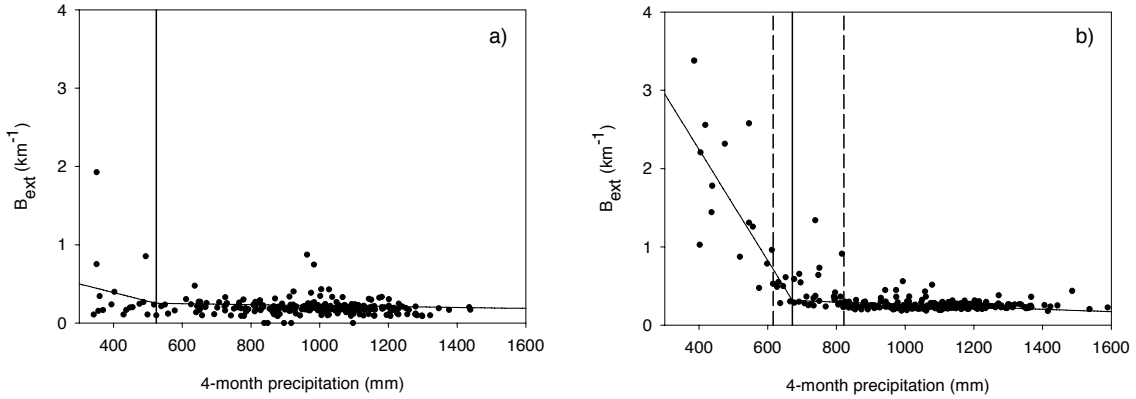

Figure S2. Kalimantan piecewise regression fits for a) 1960-1983 and b) 1984-2006. The solid vertical lines shows the threshold estimate and the dashed lines show 95% confidence intervals. This is the same data as in Figure 3, but in a scatterplot view. The threshold estimate for 1960-1983 was not well-constrained and confidence intervals are not shown.

DOI: 10.1038/NGEO443

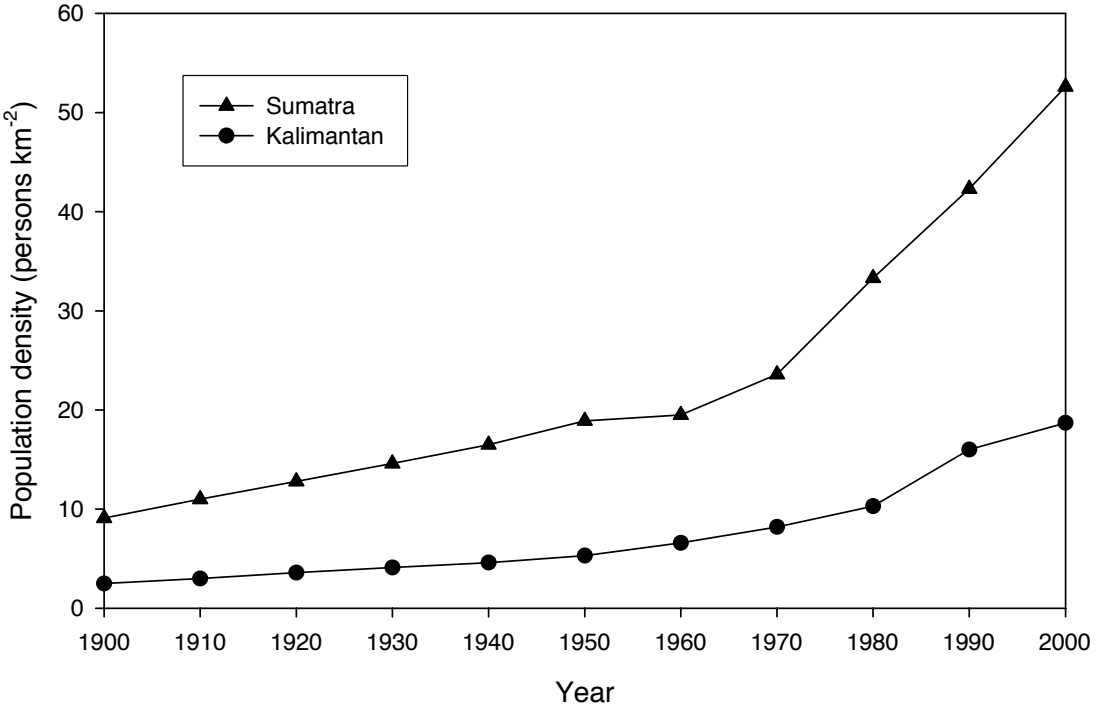

Figure S3. Population density in the southern Sumatra and southern Kalimantan analysis regions, from HYDE database [53].

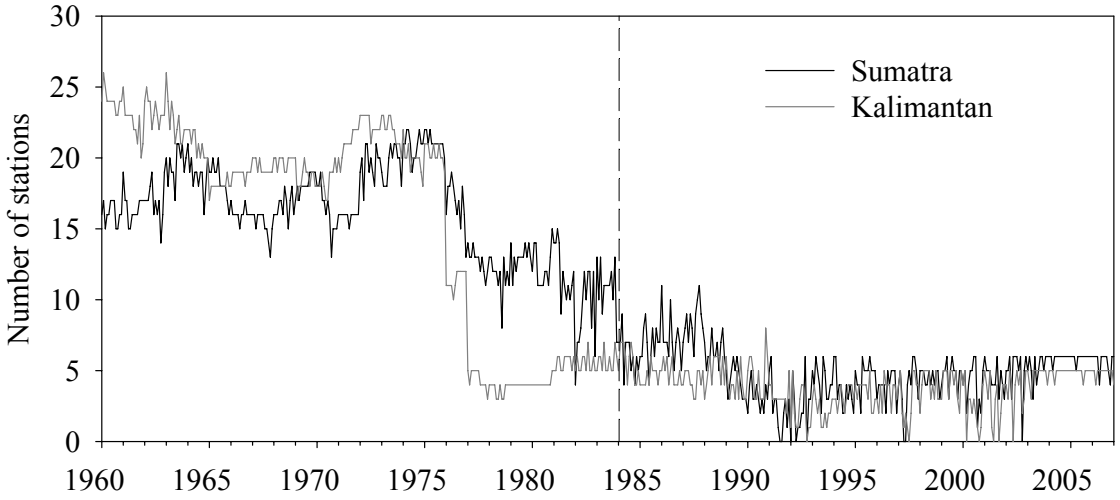

Figure S4. Monthly PRECL precipitation station counts for Kalimantan and Sumatra.

DOI: 10.1038/NGEO443

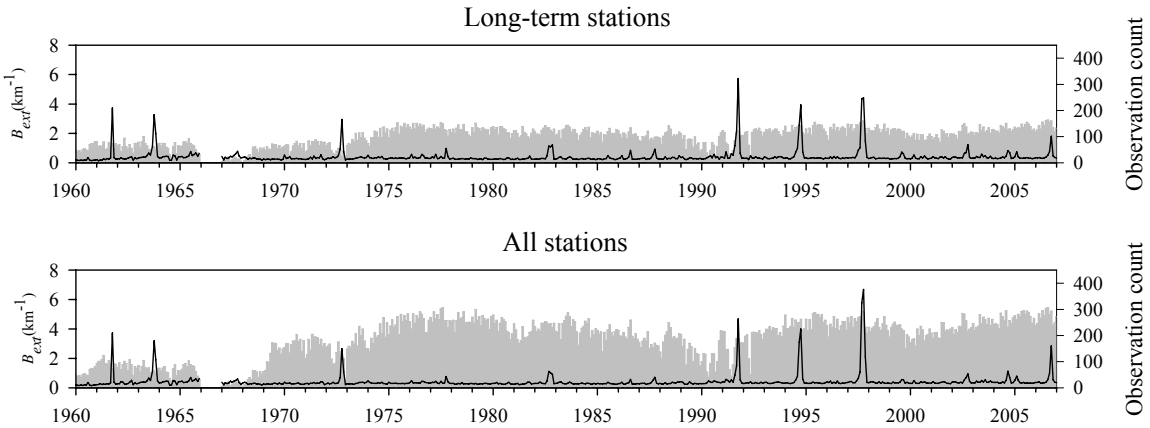

Figure S5. Regional B_{ext} for Sumatra using the long-term stations only (top) and all available stations (bottom). The solid black line shows the B_{ext} and the vertical grey bars show the number of observations.

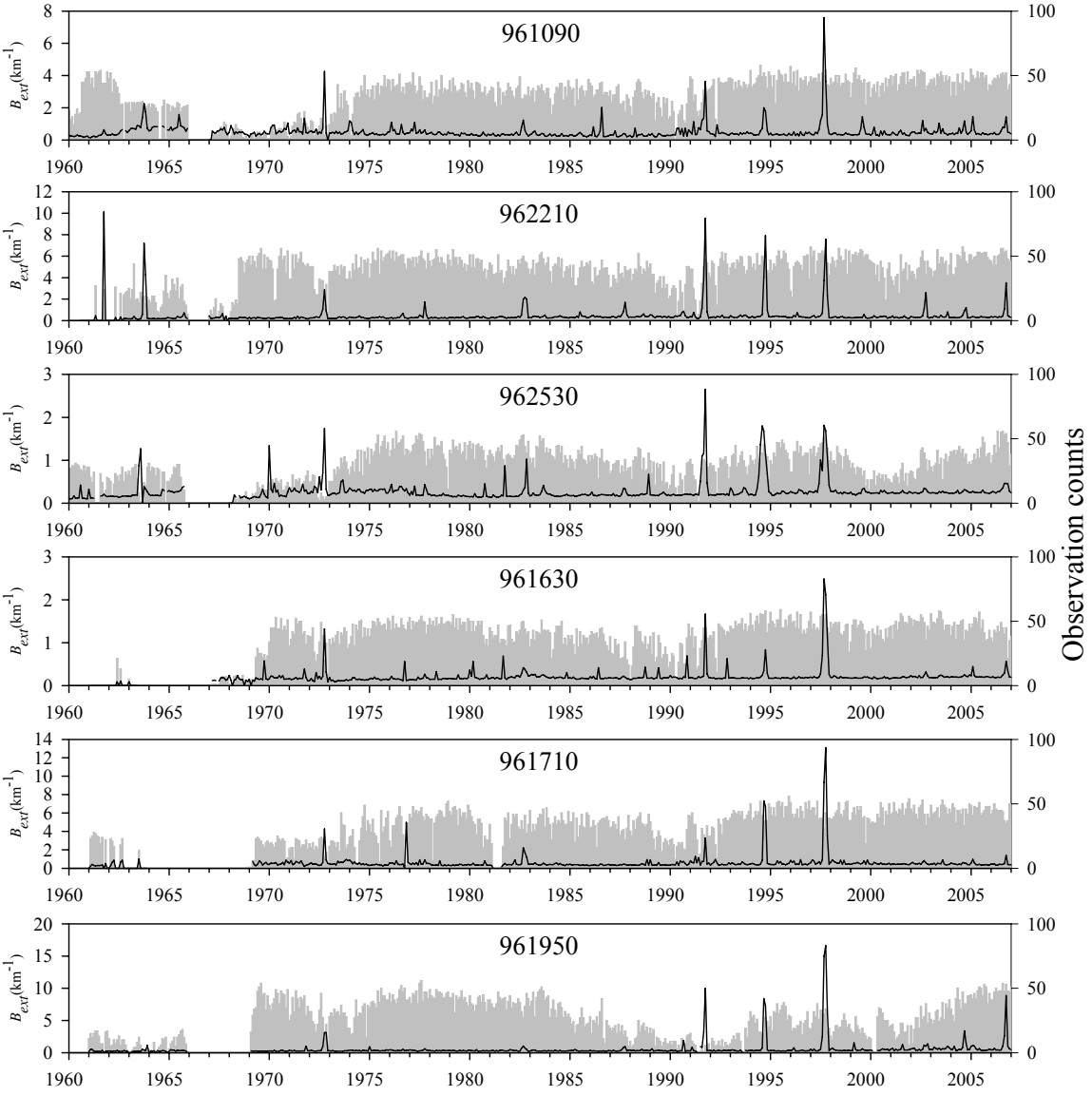

Figure S6. B_{ext} for individual stations in Sumatra. The solid black line shows the B_{ext} and the vertical grey bars show the number of observations.

DOI: 10.1038/NGEO443

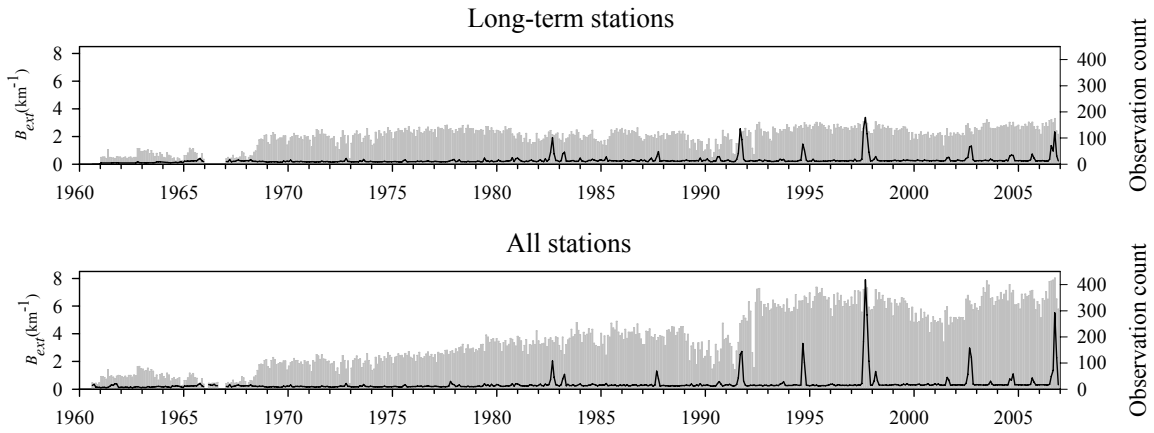

Figure S7. Regional B_{ext} for Kalimantan using the long-term stations only (top) and all available stations (bottom). The solid black line shows the B_{ext} and the vertical grey bars show the number of observations.

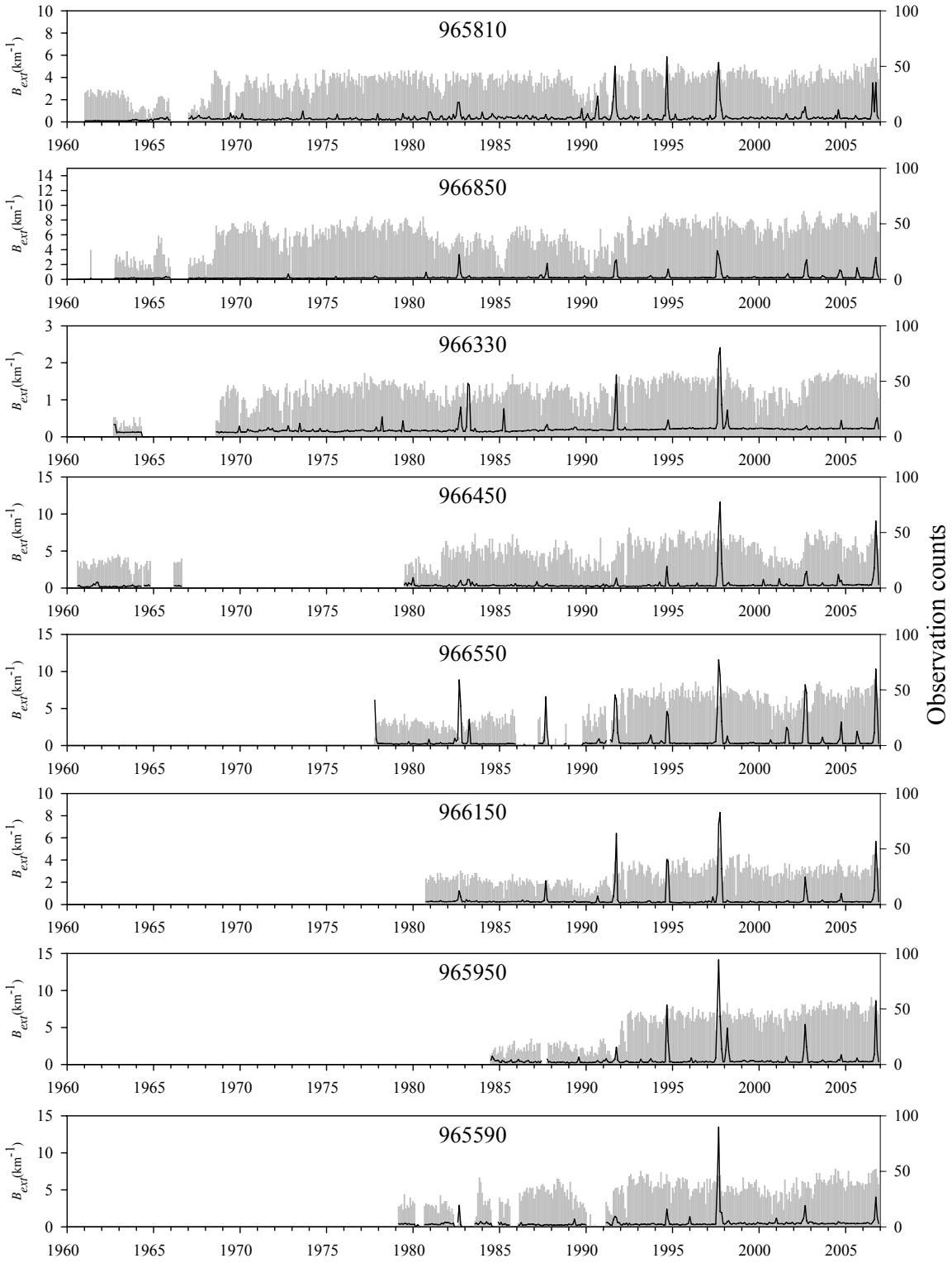

Figure S8. B_{ext} for individual stations in Kalimantan. The solid black line shows the B_{ext} and the vertical grey bars show the number of observations.

DOI: 10.1038/NGEO443

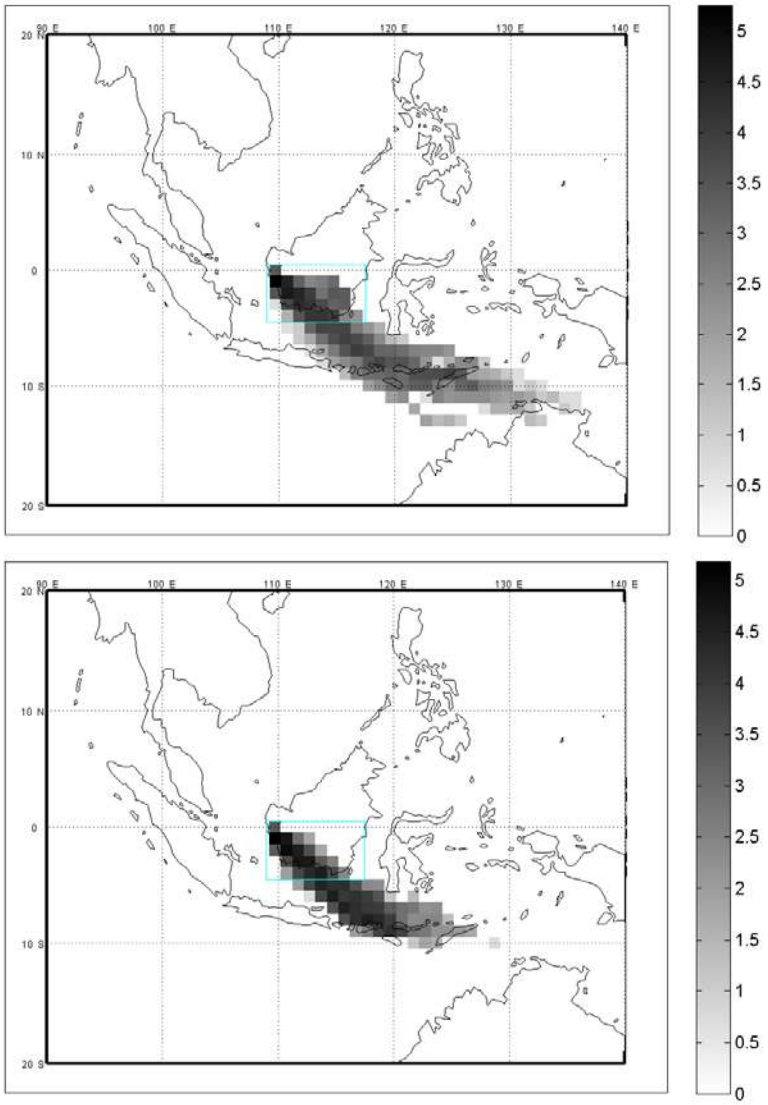

Figure S9. Pontianak back trajectory density count maps for September of 1972 (top) and 1997 (bottom). The shaded areas show the density of trajectory points on a logarithmic scale, where darker areas represent areas more frequently crossed by air masses arriving at Pontianak. The blue box outlines the same Kalimantan analysis region in Figure 1.

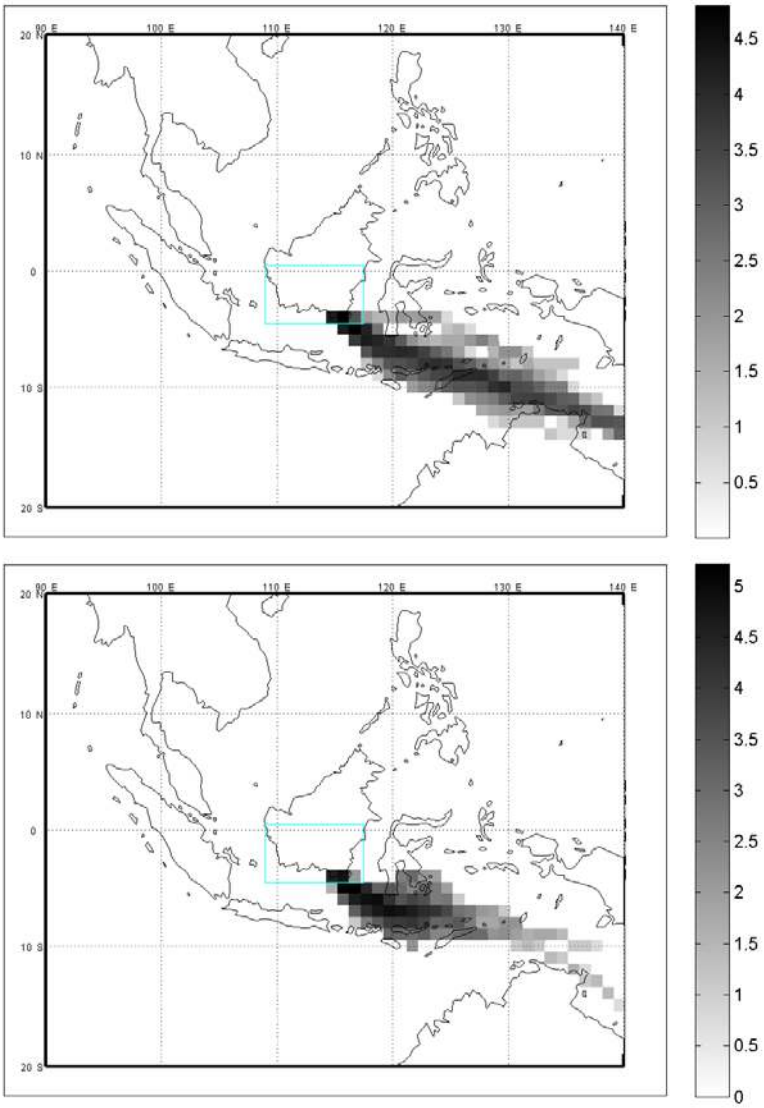

Figure S10. Banjarmasin back trajectory density count maps for September of 1972 (top) and 1997 (bottom). The shaded areas show the density of trajectory points, on a logarithmic scale, where darker areas represent areas more frequently crossed by air masses arriving at Pontianak. The blue area outlines the same Kalimantan analysis region in Figure 1.

DOI: 10.1038/NGEO443

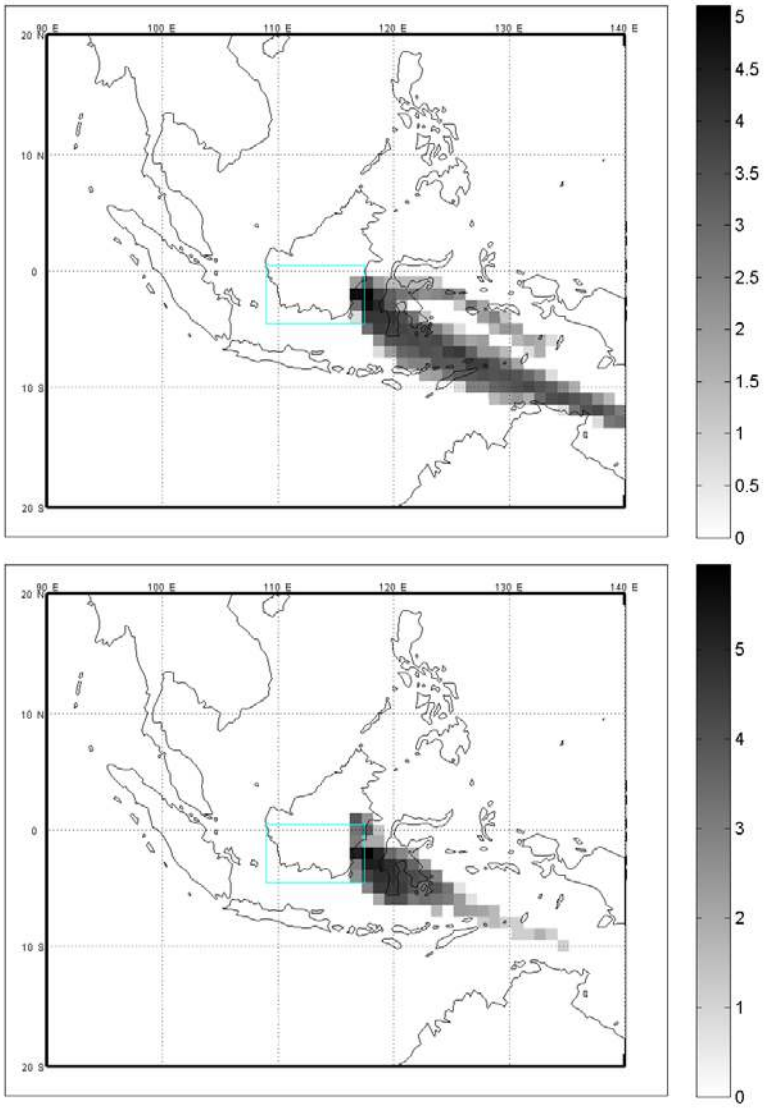

Figure S11. Balikpapan back trajectory density count maps for September of 1972 (top) and 1997 (bottom). The shaded areas show the density of trajectory points, on a logarithmic scale, where darker areas represent areas more frequently crossed by air masses arriving at Pontianak. The blue area outlines the same Kalimantan analysis region in Figure 1.